

# **Slip Tendency Analysis of Fracture Networks to Determine Suitability of Candidate Testbeds for the EGS Collab Hydroshear Experiment**

Ankush Singh, Ghanashyam Neupane,  
Pat Dobson, Mark Zoback, Joseph  
Morris, Pengcheng Fu, Paul Schwering,  
William Roggenthen, Luke Frash, Tim  
Kneafsey, Martin Schoenball, Yves  
Guglielmi, Hunter Knox, Craig Ulrich,  
Nuri Uzunlar, Tom Doe, Herb Wang,  
Kate Condon, Bud Johnston

The INL is a U.S. Department of Energy National Laboratory  
operated by Battelle Energy Alliance



September 2019



The INL is a U.S. Department of Energy National Laboratory  
operated by Battelle Energy Alliance

# **Slip Tendency Analysis of Fracture Networks to Determine Suitability of Candidate Testbeds for the EGS Collab Hydroshear Experiment**

**Ankush Singh, Ghanashyam Neupane, Pat Dobson, Mark Zoback, Joseph Morris, Pengcheng Fu, Paul Schwering, William Roggenthen, Luke Frash, Tim Kneafsey, Martin Schoenball, Yves Guglielmi, Hunter Knox, Craig Ulrich, Nuri Uzunlar, Tom Doe, Herb Wang, Kate Condon, Bud Johnston**

**September 2019**

**Idaho National Laboratory  
Idaho Falls, Idaho 83415**

**<http://www.inl.gov>**

**Prepared for the  
U.S. Department of Energy  
Office of Energy Efficiency and Renewable Energy  
Under DOE Idaho Operations Office  
Contract DE-AC07-05ID14517**

# **Slip Tendency Analysis of Fracture Networks to Determine Suitability of Candidate Testbeds for the EGS Collab Hydroshear Experiment**

**Ankush Singh and Mark Zoback**  
*Stanford University, Stanford California, USA*

**Ghanashyam Neupane**  
*Idaho National Laboratory, Idaho Falls, Idaho, USA*

**Patrick F. Dobson, Timothy J. Kneafsey, Martin Schoenball, Yves Guglielmi and Craig Ulrich**  
*Lawrence Berkeley National Laboratory, Berkeley, California, USA*

**William Roggenthen and Nuri Uzunlar**  
*South Dakota School of Mines and Technology, Rapid City, South Dakota, USA*

**Joseph Morris and Pengcheng Fu**  
*Lawrence Livermore National Laboratory, Livermore, California, USA*

**Paul C. Schwering and Hunter A. Knox**  
*Sandia National Laboratories, Albuquerque, New Mexico, USA*

**Luke Frash**  
*Los Alamos National Laboratory, Los Alamos, New Mexico, USA*

**Thomas W. Doe**  
*TDoeGeo, Redmond, Washington, USA*

**Herb Wang and Kate Condon**  
*University of Wisconsin, Madison, Madison, Wisconsin, USA*

**Bud Johnston**  
*National Renewable Energy Laboratory, Golden, Colorado, USA*

**The EGS Collab Team<sup>1</sup>**  
*Multiple affiliations*

---

<sup>1</sup> J. Ajo-Franklin, T. Baumgartner, K. Beckers, D. Blankenship, A. Bonneville, L. Boyd, S. Brown, S.T. Brown, J.A. Burghardt, T. Chen, Y. Chen, K. Condon, P.J. Cook, D. Crandall, P.F. Dobson, T. Doe, C.A. Doughty, D. Elsworth, J. Feldman, A. Foris, L.P. Frash, Z. Frone, P. Fu, K. Gao, A. Ghassemi, H. Gudmundsdottir, Y. Guglielmi, G. Guthrie, B. Haimson, A. Hawkins, J. Heise, M. Horn, R.N. Horne, J. Horner, M. Hu, H. Huang, L. Huang, K.J. Im, M. Ingraham, R.S. Jayne, T.C. Johnson, B. Johnston, S. Karra, K. Kim, D.K. King, T. Kneafsey, H. Knox, J. Knox, D. Kumar, K. Kutun, M. Lee, K. Li, Z. Li, R. Lopez, M. Maceira, P. Mackey, N. Makedonska, C.J. Marone, E. Mattson, M.W. McClure, J. McLennan, T. McLing, C. Medler, R.J. Mellors, E. Metcalfe, J. Miskimins, J. Moore, C.E. Morency, J.P. Morris, S. Nakagawa, G. Neupane, G. Newman, A. Nieto, C.M. Oldenburg, W. Pan, T. Paronish, R. Pawar, P. Petrov, B. Pietzyk, R. Podgorney, Y. Polsky, J. Pope, S. Porse, B.Q. Roberts, M. Robertson, W. Roggenthen, J. Rutqvist, D. Rynders, H. Santos-Villalobos, M. Schoenball, P. Schwering, V. Sesetty, C.S.

## Keywords

*EGS Collab, Shear Stimulation, Slip Potential, Site Selection*

## ABSTRACT

Experiment 2 of the EGS Collab project is aimed at testing stimulation by hydro-shearing of existing natural fractures, versus Experiment 1, which is focused on hydraulic fracturing a rock mass to enhance permeability. The main criterion for the testbed selection in Experiment 2 is the presence of an interconnected network of fractures, at least 10 meters in extent, and with orientations such that shear slip can be induced at injection pressures less than the minimum horizontal stress ( $S_{hmin}$ ). The feasibility analysis for this experiment requires a well-constrained stress state along with well-characterized fracture networks. The fracture systems at two candidate locations in the Sanford Underground Research Facility (SURF), the 4850 Level (number refers to depth below ground surface in feet) and the 4100 Level, have been characterized to different extents. The 4850 Level has a well-characterized Discrete Fracture Network (DFN) from borehole (drilled for an experimental test bed) and drift observations. In contrast, the 4100 level has a fracture network characterized only by observations from the drift wall, which provides little constraint on fracture extents. This paper will present assessments for the interpreted slip potential for the natural fractures at the two locations. Data uncertainties are addressed by performing a probabilistic analysis that takes into account the uncertainty in the stress state, uncertainty in the fracture properties, and preliminary borehole locations. There is strong evidence of shear stimulation of some natural fractures in Experiment 1 on the 4850 level. We use examples of natural fractures strongly linked to shear stimulation in Experiment 1 from multiple monitoring indicators to test the consistency of the stress model and guide the uncertainty interpretation. This analysis is intended to guide the site selection process for Experiment 2 by highlighting the fracture orientations that are likely to be shear-stimulated in a majority of modeled realizations.

## 1. Introduction

The EGS Collab Project is aimed at using fluid injection experiments at the Sanford Underground Research Facility (SURF) in Lead, South Dakota to understand the response of crystalline rocks to stimulation at the decameter scale (Kneafsey et al., 2019a, b; Dobson et al., 2018). A more detailed description of the experiments is given by Kneafsey et al. (2019b).

Following Experiment 1, which was aimed at understanding tensile hydraulic fracturing in crystalline rocks, Experiment 2 of the EGS Collab project aims to test the shear stimulation of natural fractures in response to fluid injection (Kneafsey et al., 2019b, Dobson et al., 2018). The overall objectives of Experiment 2, i.e. the hydroshear experiment, are given in details by Dobson et al. (2018). These include:

1. Shear stimulation of natural fractures between two boreholes ~10 m apart.

---

Sherman, A. Singh, M.M. Smith, H. Sone, F.A. Soom, P. Sprinkle, C.E. Strickland, J. Su, D. Templeton, J.N. Thomle, C. Ulrich, N. Uzunlar, A. Vachaparampil, C.A. Valladao, W. Vandermeer, G. Vandine, D. Vardiman, V.R. Vermeul, J.L. Wagoner, H.F. Wang, J. Weers, N. Welch, J. White, M.D. White, P. Winterfeld, T. Wood, S. Workman, H. Wu, Y.S. Wu, Y. Wu, E.C. Yildirim, Y. Zhang, Y.Q. Zhang, Q. Zhou, M.D. Zoback

2. Testing the flow behavior of the stimulated fractures through tracer tests and long term thermal tests.
3. Understanding the effects of stimulation on permeability enhancement and thermal performance of Enhanced Geothermal (EGS) reservoirs.
4. Constraint on numerical models with test monitoring data.

The first step to Experiment 2 is to identify a suitable test bed. In order to perform an interpretable and well monitored shear stimulation experiment, the following geological criteria have been identified for a potential testbed location:

1. Presence of natural fractures or fracture zone at least 10 meters in length and appropriate orientation for shear failure.
2. ‘Goldilocks permeability’; i.e., high enough for a pre-stimulation flow test but low enough to have sufficient permeability enhancement in response to shear stimulation
3. Multiple candidates in the testbed for stimulation.
4. Test-bed with a well characterized stress state and well described fracture network.
5. Low likelihood of leak-off through intersection with other permeable features or into the drift.
6. Low heterogeneity in order to facilitate interpretation of geophysical signals (e.g., microseismic monitoring and time-lapse electrical resistivity tomography (ERT))

Selection of an appropriate site is one of the most important activities in the success of Experiment 2. Two candidate sites have been identified as the potential locations for Experiment 2 (Dobson et al., 2018). This paper aims to capture the current understanding about the candidate sites for the hydroshear experiment with an emphasis on the presence of natural fractures that are optimally oriented for shear stimulation.

## **2. Candidate Site Geological Parameters**

The two candidate sites for Experiment 2 are situated in the 4850 and 4100 levels at SURF. The sites have significant differences, particularly in terms of the in-situ geological characteristics and the degree of characterization. The potential site on the 4850 level (4850L) is located in the carbonate-rich, quartz-bearing phyllite of the upper Poorman formation (Caddey et al., 1991), and has been locally very well characterized by the KISMET project (Oldenburg et al., 2017) and EGS Collab Experiment 1 (Kneafsey et al., 2019a). The candidate site on the 4100 level (4100L) is located in the Yates amphibolite (Caddey et al., 1991) and has not yet been characterized with the granularity of the 4850L site. This site is located in the proximity of a battery charging alcove about 200 feet south of the Yates shaft (Dobson et al., 2018).

A number of non-geological aspects play an important role in candidate site selection. These include physical drift conditions, availability of appropriate facilities such as power requirements, water disposal, material transport facilities, etc. Some of these criteria are discussed by Dobson et al. (2018).

## 2.1 Stress State

The stress state at the 4850 level is well characterized with vertical well stress measurements conducted as a part of the kISMET project (Wang et al., 2017). The site is in a normal to strike-slip faulting regime with both optimally normal and strike-slip faults expected to be activated with increase in pore pressure. The stress state of the 4850 level has been constrained from the following analysis:

1. Vertical Stress ( $S_v$ ): The vertical stress ( $S_v$ ) has been computed for a reference depth of 1478 m (4850 feet) using the relation proposed by Pariseau (1986). This analysis is in good agreement with the overburden density estimates from Hart et al. (2014).
2. Minimum horizontal stress ( $S_{hmin}$ ):  $S_{hmin}$  magnitude and orientation have been estimated from vertical well hydraulic fracture experiments in the kISMET wells (Wang et al., 2017, Ulrich et al., 2018, Dobson et al., 2018).
3. Maximum horizontal stress ( $S_{Hmax}$ ):  $S_{Hmax}$  magnitude for the site has been estimated using a wellbore breakout analysis in which the presence and absence of borehole breakouts in three closely spaced wells of different orientations was compared to forward models with different values of  $S_{Hmax}$  as a function of  $S_v$ . Figure 1a shows the relative locations of three boreholes: borehole-D, borehole-J and kISMET vertical well, used for the analysis. Borehole breakouts were observed from televiewer log data in borehole-J, while the other two boreholes did not experience any breakouts. Assuming the rock strength to be constant for the three boreholes, these observations are consistent with rock failure forward models for:  $S_{Hmax} \cong 0.8 - 0.9 \times S_v$ . For a higher  $S_{Hmax}$  magnitude, the likelihood for the vertical kISMET well to experience borehole breakouts increases relative to the borehole-J, while for a lower  $S_{Hmax}$  magnitude, borehole-D has a higher likelihood of experiencing borehole breakouts.  $S_{Hmax}$  magnitude is the biggest uncertainty amongst the stress parameters.

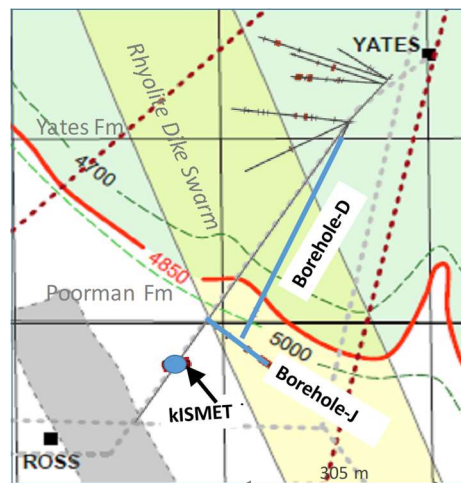


**Figure 1.** The horizontal boreholes used for the breakout analysis are indicated by the blue lines (borehole-D and borehole-J). The vertical well location is indicated by the blue ellipse (kISMET). The boreholes are located in close vicinity and the presence/absence of borehole breakouts is attributed to their orientations.

No borehole breakouts have been observed in the boreholes drilled in Experiment 1 at the 4850 candidate site. The lack of breakouts in the nominally N-S oriented injection,

production and monitoring boreholes is consistent with the  $S_{Hmax}$  analysis for the three boreholes described. However, the lack of borehole breakout observations in the nominally E-W oriented monitoring boreholes might be indicative of either a variation in rock strength or a stress perturbation related to the presence of a rhyolite dyke swarm in the area of borehole-J. A large uncertainty in  $S_{Hmax}$  magnitude is considered in the probabilistic analysis to reflect these observations.

4. Pore pressure measurements have indicated pore pressures significantly below hydrostatic pressure, influenced by multiple pumping and flooding events related to the mining activities. The reference pore pressure used for the present analysis is the maximum expected reservoir pressure reported by Stetler (2015). Significant pore pressure variations are expected over short distances for the site locations. The uncertainty in the initial pore pressure is not significant for this analysis as the slip tendency is described for maximum injection pressures equal to the least principal stress, which is independent of initial pore pressure.

Table 1 summarizes the stress state information for the 4850 candidate site.

**Table 1 Stress parameters used in the analysis (adapted from Dobson et al., 2018)**

Parameter	Input value	Stress/Pressure gradient
$S_V$	6062 psi	1.25 psi/ft
$S_{hmin}$	3147 psi	0.65 psi/ft
$S_{Hmax}$ azimuth	85°	n.a.
$S_{Hmax}$	4931 psi	1.02 psi/ft
Pore pressure ( $P_p$ )	1200 psi	0.25 psi/ft
Friction coefficient ( $\mu$ )	0.6	n.a.

In contrast, the state of stress for the 4100 level is relatively unconstrained. A stress measurement campaign is planned for the 4100 level for the summer of 2019. For the present analysis, the relative stress magnitudes and stress orientations at the 4100 level have been assumed to be the same as the 4850 level. The stress gradients reported in Table 1 have been used for a reference depth of 4100 feet to project the stress magnitudes to the 4100 candidate site.

White et al. (2017) showed that the thermal stresses from the drift might result in a significant perturbation close to the drift wall. For the present analysis, we only consider far field stresses and ignore the effects of the near drift thermal stress perturbations.

## **2.1 Fracture Characterization**

### **2.1.1 DFN characterization of the 4850 site**

If Experiment 2 were to be conducted on the 4850L, it would be performed at (or very near) the Experiment 1 testbed. In the early stages of the experiment, there was a significant effort to define a ‘common’ discrete fracture network (DFN) based on preliminary hydraulic characterization efforts of natural fractures encountered in the testbed (Schwering et al., 2018). The interpretive focus was on identification of fractures that 1) had demonstrable or likely connectivity between the wells drilled for Experiment 1 and 2) may have implications/effects on Experiment 1 hydraulic

stimulation/flow testing. The analysis indicated the presence of at least three semi-vertical, northwest-oriented fracture zones in the testbed (Figure 2). This initial common DFN model is evolving and being refined as stimulation/flow testing and geophysical monitoring provide further insights on hydraulic connectivity among the fractures.

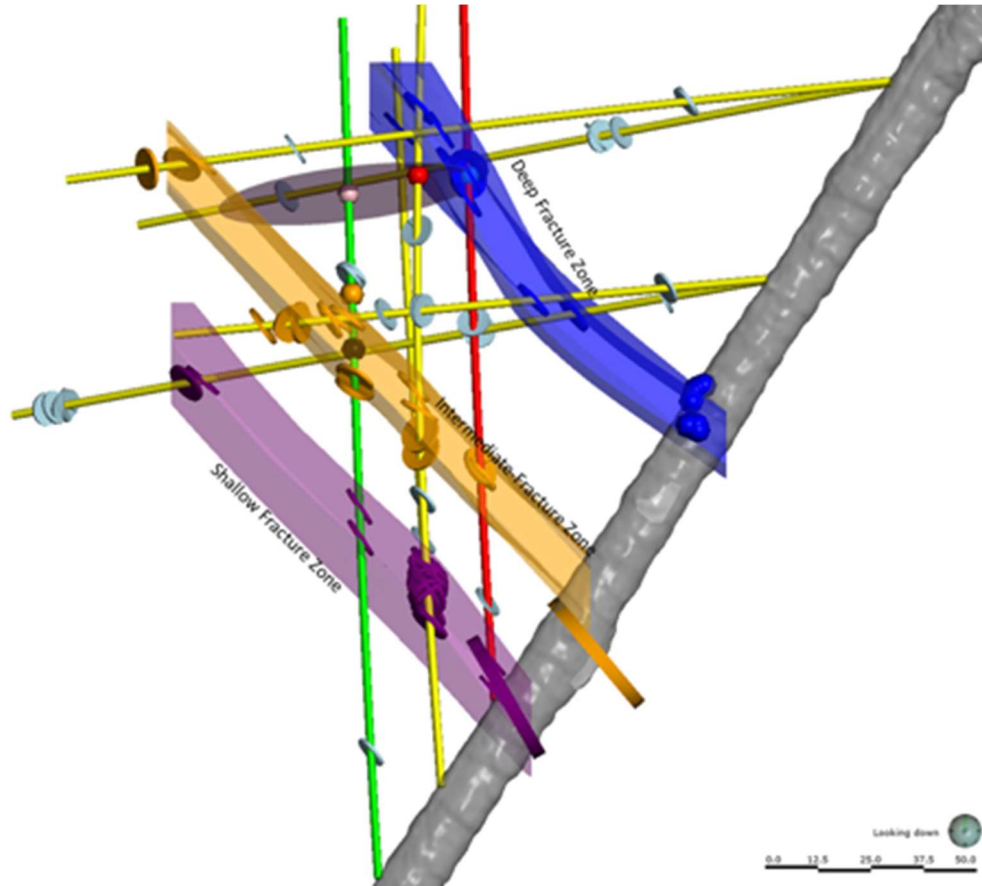


**Figure 2: Common DFN (map view) of the Experiment 1 testbed. The 4850L drift is represented by the thick grey tube, and the Experiment 1 wells are indicated by thin multicolored tubes. Note 3 inferred fracture zones based on initial hydraulic characterization of natural fractures encountered in the testbed (multicolored discs). The grey, semi-transparent disc represents a hydraulic stimulation target.**

### 2.1.2 4100 Drift wall mapping of fractures

The fracture characterization for the 4100 site is restricted to mapping of features along the drift wall. The drift mapping has focused on the proposed site near the battery charging alcove south of the Yates shaft. The observed fractures can be classified into three main groups: 1) Joint set 2 (JS2) having large Tertiary fractures with evidence of shearing; 2) Joint set 1 (JS1) having mostly foliation/fabric-parallel features; 3) and joint set 3 (JS3) and scattered small width healed fractures that may be possibly conjugate shear sets. The large Tertiary fractures are characterized by cement fillings consisting of calcite, quartz and gypsum and observations of unfilled openings. These fractures are laterally continuous and might be the most suitable targets for shear stimulations. Figure 3a shows a stereogram of the poles of all the planar features mapped for the 4100 level. The large fractures have a characteristic ~E-W strike and near vertical dip. Figure 3b shows an example of a large Tertiary fracture mapped on the drift wall.

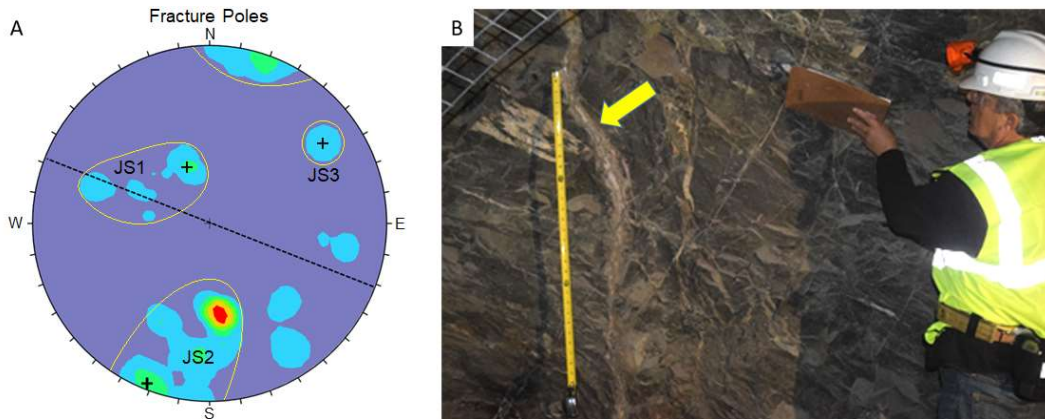


**Figure 3 a. Stereogram of poles of all features and fractures on the 4100. The crosses show the orientation of the dominant fracture sets (JS1, JS2, and JS3) and the dashed line shows the orientation of the nearly vertical fractures striking to the northwest (JS2); b. Large Tertiary fracture (denoted by yellow arrow) near the tape measure for scale (intervals on the tape are 1 ft). The fracture is filled in this photograph but other, similar fractures are exposed in the drift have open space.**

## 2.2 Site Lithology

The two sites being considered for the next phase of the project consist of the currently developed location on the 4850 Level and a candidate site on the 4100 Level. Although both are hosted in Poorman Formation, they are located in two significantly different lithological units. The 4850 site is hosted in the metasedimentary phyllite of the upper Poorman Formation referred to as the Ross Member by Steadman and Large (2016), and the 4100 site is in the amphibolite of the Yates Unit (informal unit of Caddey et al., 1991). The Ross Member at this location is a graphitic carbonate mica phyllite with abundant quartz and calcite veins that is intensely deformed by mesoscale folding. The Yates Unit is an amphibolite metabasalt consisting of hornblende and plagioclase (Caddey et al., 1991, Neupane et al., 2019).

Condon et al. (2018) describe the effects of foliation and heterogeneity on the rock properties for the Poorman phyllite at the 4850 test site. The elastic properties and sonic velocities show a significant dependence on orientation with respect to the foliation planes and the degree of folding observed in the samples. The experiments found a large variation in Uniaxial Compressive Strength (UCS) between different samples from nearby locations with a range from 25-195 MPa. Frash et al. (2019) also observed strong anisotropy for shear waves with S-wave velocity varying between 4240 m/s parallel to the foliation planes to 1260 m/s for high angles to the foliation planes. The measured permeability for the intact formation is less than  $1\mu D$  (Frash et al., 2019), indicating that there is likely to be negligible contribution from matrix flow during the injection experiments. There are no rock property measurements available for the Yates amphibolite at the 4100 level. Previous measurements of rock properties summarized by Vigilante (2016) indicate that the UCS is higher from the amphibolite samples compared to the phyllite samples. Also, the Yates amphibolite is less heterogeneous on the outcrop scale compared to the Poorman phyllite.

While, on the basis of the current knowledge of the rock properties, it is difficult to distinguish between the two candidate sites, the seemingly lower heterogeneity in the Yates amphibolite may lower the complexity in interpretation of geophysical signals.

### 3. Slip Tendency Analysis

The purpose of the slip tendency analysis is to delineate the fracture orientations optimally oriented for shear slip. For a shear stimulation experiment, the injection must be performed in an interval that includes optimally oriented fractures with a high probability of being a part of an interconnected fracture network such that enhanced flow pathways can result from shear slip induced permeability enhancement. The ideal location will have a number of fractures in close proximity that have a high probability of being potentially active in response to fluid injection.

#### 3.1 4850 Level

Slip tendency analysis for the mapped fractures has been performed using the Fault Slip Potential (FSP) tool (Walsh et al., 2017). The shear stimulation is described by the well-established Coulomb failure criterion:  $\tau = \mu\sigma_n$ , where  $\tau$  is the shear stress acting on the fracture plane,  $\mu$  is the coefficient of sliding friction and  $\sigma_n = S_n - P_p$  is the effective normal stress acting on the fault plane where  $S_n$  is the total stress and  $P_p$  is the pore pressure, we compute the effective normal and shear stresses acting on the observed planes. The pore pressure increment required to cause failure for the fracture planes is then computed by calculating the pore pressure required for a positive value of the Coulomb failure function (CFF):  $\tau - \mu\sigma_n$ .

The fracture planes for which shear failure is predicted at lower pressure than a hydraulic fracture pressure are classified as high fault slip potential and fractures in which shear failure is not expected at hydraulic fracture pressures are classified as low fault slip potential. We assume zero tensile strength of the rock for these conditions. It is important to note that the Coulomb criterion does not make a distinction regarding whether the failure is aseismic or seismic.

Figure 4 shows a summary of the failure analysis for all the fractures mapped in the DFN characterization for the 4850 level. The red fractures plotted in both a Mohr circle and a stereo-net representation are optimally oriented for failure. Near-vertical fractures striking at low angles to  $S_{Hmax}$  are the most likely to be shear stimulated. There seems to be distinct set of mapped NW-SE striking fractures with a high shear stimulation potential at the 4850 level. The orange rectangle in the figure represents fracture orientations sub-parallel to  $S_{Hmax}$ , which have the potential for both opening and shear failure.

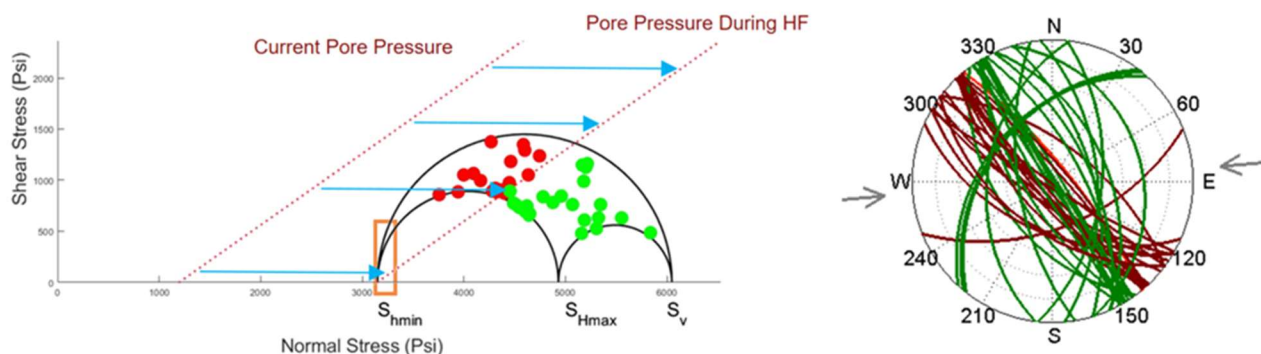


**Figure 4: Shear slip potential for fractures characterized as a part of the DFN exercise (Figure 2) plotted with a Mohr-circle representation (left) and a stereo-net (right). Red color indicates fractures that are likely to be shear stimulated, while green fractures are stable fractures. The orange region indicates fracture orientations parallel to  $S_{Hmax}$  that have dilation potential.**

### 3.2. 4100 Level

The fracture characterization for the 4100 level is limited compared to the 4850 level due to the lack of borehole data. Dobson et al. (2018) described the shear slip analysis for fractures characterized from a limited mapping of the drift wall. We have performed a shear slip analysis on an updated fracture interpretation from the drift exposures following a comprehensive fracture mapping exercise. The 4100 shear slip analysis reveals a distinct set of E-W trending planes (JS2) that have extremely high shear slip potential with orientations nearly parallel to  $S_{Hmax}$  (Figure 5). These fractures are at an optimal orientation for dilation as this is close to the orientation with the least normal stress component. The fractures denoted by the red star and green triangle are representative of the large Tertiary fractures and sulfide layers parallel to the foliation respectively. The large Tertiary fractures are optimally oriented for shear slip and could be feasible targets for shear stimulation. It should be noted however that the high proportion of favorable orientations to shear slip might be exaggerated due to bias in sampling features that are at a high angle to the drift wall.

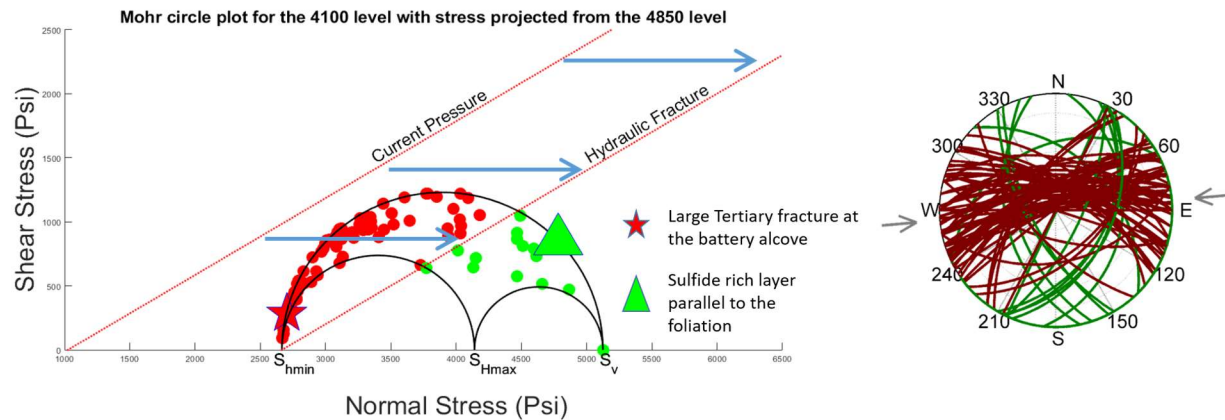


**Figure 5** Shear slip potential for fractures mapped from the 4100 drift wall plotted with a Mohr-circle representation (left) and a stereo-net (right). The colors are the same as Figure 4.

#### 3.2.1 Not all fractures predicted to fail

One of the important outcomes of the failure analysis is the recognition that not all fracture planes can undergo opening mode (dilate) or shear failure irrespective of the fluid injection set-up in the experiment. In addition to the orientations that can undergo shear slip, a very narrow range of fracture orientations can undergo both opening mode and shear failure. These are the fracture orientations sub-parallel to  $S_{Hmax}$ , i.e., orientations with the lowest normal stress acting on them. A number of examples for different stress configurations are presented by Zoback and Lund-Snee (2018).

For the stress state at the 4850 level, certain orientations, for example fractures at high angle to  $S_{Hmax}$  or near horizontal fractures will not undergo shear slip failure even after considering a large  $S_{Hmax}$  uncertainty. This is an important consideration that can be used to constrain interpretation of planes formed by alignment of micro-earthquakes (MEQs) during microseismic monitoring. Figure 6 shows an example of such a plane with a shallow dip of  $25^\circ$  striking at a high angle from

$S_{Hmax}$  denoted by the blue star on the Mohr circle plots. We consider a wide  $S_{Hmax}$  uncertainty ranging from  $0.6 \times S_v$  to  $S_v$  and show that a misoriented plane plots far away from the failure line in all the cases.

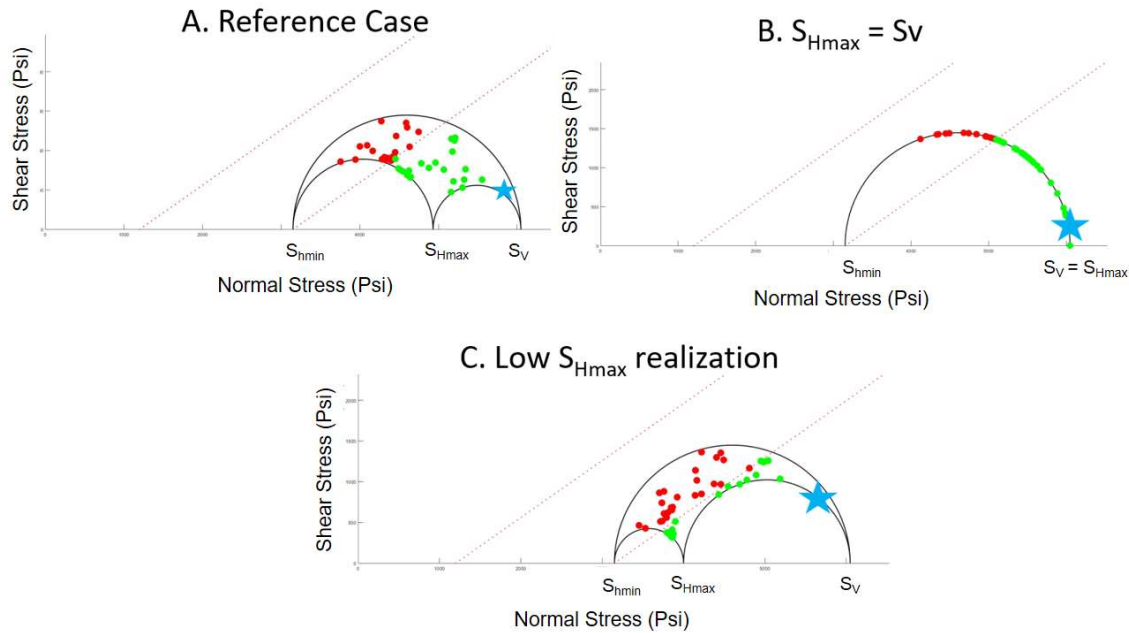


**Figure 6.** The position of a misoriented fracture plotted on Mohr circle diagrams assuming  $S_{Hmax}$  varying from reference case:  $0.8 \times S_v$  (A), high case:  $S_{Hmax} = S_v$  (B), low case:  $S_{Hmax} = 0.6 \times S_v$  (C). The misoriented fracture is a shallow dipping fracture striking at a high angle to  $S_{Hmax}$ . The fracture remains stable in the context of Coulomb failure in response to fluid injection even after considering the maximum  $S_{Hmax}$  uncertainty range.

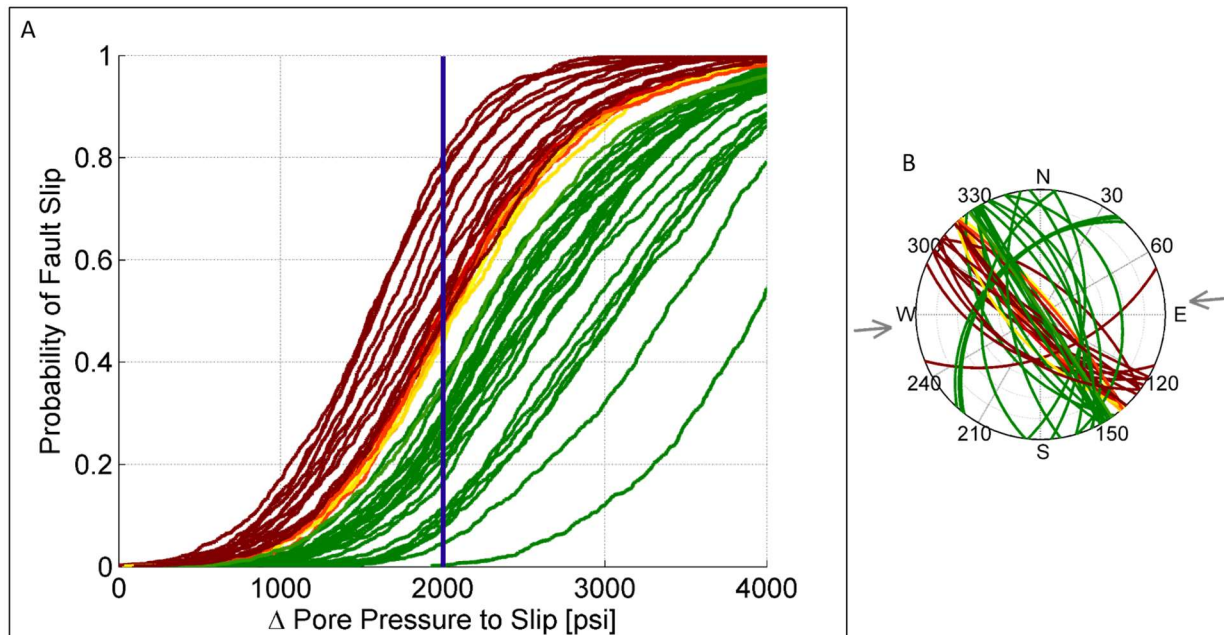
### 3.3 Probabilistic Analysis

A number of the input parameters such as  $S_{Hmax}$  magnitude have a high associated uncertainty. A probabilistic analysis is performed to take into account the uncertainties in all the input parameters including fracture orientations, stress orientation and principal stress magnitudes. The ranges of the input parameters for the 4850 site are described in Table 2.

**Table 2.** Summary of the uncertainty range for all parameters considered in the probabilistic analysis. The uncertainty range is added to the reference case values summarized in Table 1.

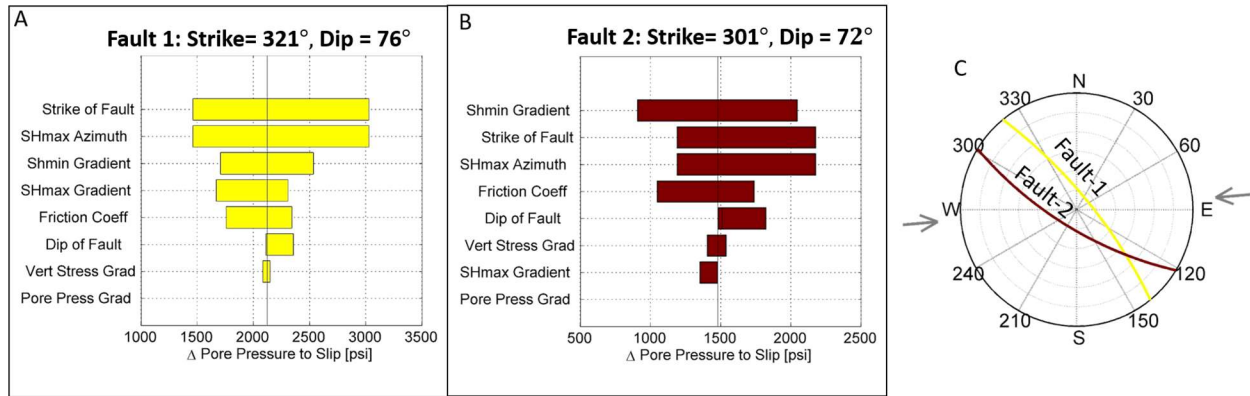
Parameter	Uncertainty range ( $\pm$ reference case value)
$S_v$ magnitude	0.1 psi/ft
$S_{hmin}$ magnitude	0.1 psi/ft
$S_{Hmax}$ magnitude	0.25 psi/ft
$S_{Hmax}$ orientation	20°
Fracture strike	20°
Fracture dip	20°
Friction coefficient	0.6-1.0

Assuming a uniform distribution of input parameters values, a Monte Carlo analysis is performed by randomly sampling these input distributions. The Monte Carlo analysis computes the probability of each fault slipping as a function of pore pressure increase. This is represented by a cumulative distribution function (CDF) for each fault plane as shown in Figure 7. The CDF describes the probability of shear failure for each plane for a given pore pressure increment. The blue line in Figure 7 indicates the pressure increment required to create a hydraulic fracture, i.e.  $S_{hmin}$  minus the current pore pressure and planes that have a probability of shear failure greater than 0.5 at this pore pressure increment are colored red. This analysis can be used to identify fracture planes that have a high probability of shear stimulation for a desirable pore pressure increment as a part of the experimental design. The methodology of the probabilistic analysis is described in detail by Walsh et al. (2017).



**Figure 7 A. Cumulative distribution function (CDF) curves for individual fracture planes mapped at the 4850 site showing the probability of slip versus the pores pressure increment. The blue vertical line indicates the hydraulic fracture condition ( $P_p = S_{hmin}$ ) and the fracture planes with a probability of shear failure greater than 0.5 at this configuration are colored red. B. Stereo-net plot showing the orientations of the fracture plotted in the CDFs. The fractures with high probability of slip at around hydraulic fracturing pressure are mostly oriented NW-SE with near vertical dip. The inward pointing arrows correspond to the reference case  $S_{Hmax}$  azimuth. This analysis can be done for any chosen pore pressure increment according to the experimental design and is useful to compare between different fractures as potential targets of shear stimulation.**

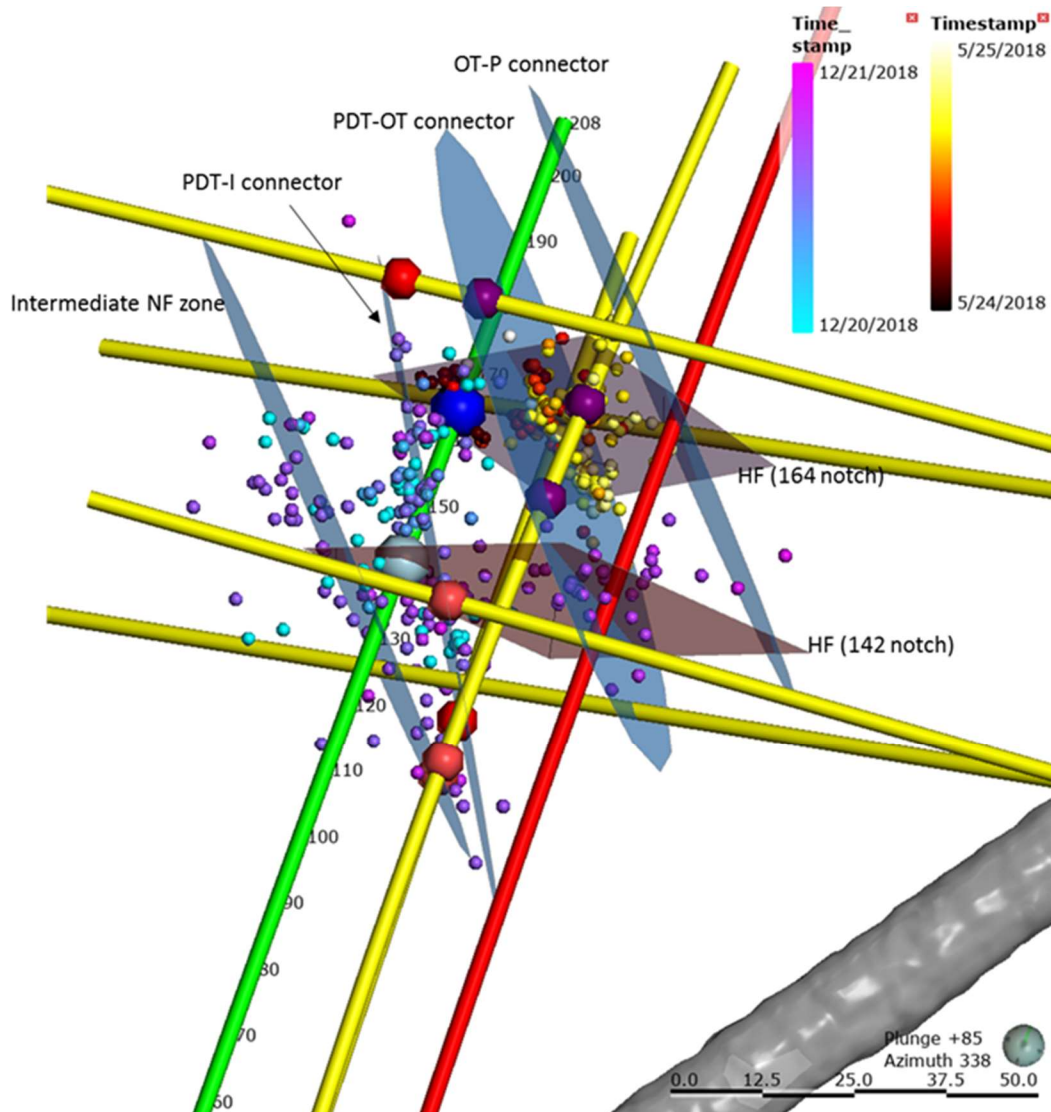
To characterize the impact of specific parameter uncertainties (as noted in Table 2) on the shear failure of a particular fracture plane, the sensitivity of pore pressure to slip for a fracture plane to each input parameter can be visualized in the form of tornado plots. Figure 8 shows an example of a tornado plot for two fractures with slightly different orientations at the 4850 site. The first fracture seems to be most sensitive to a  $\pm 10^\circ$  uncertainty in fault strike, while the second fracture is most sensitive to the variation in  $S_{hmin}$  gradient. The difference in sensitivity for the two fracture planes is due to the difference in orientation with respect to  $S_{Hmax}$ . These plots can be utilized to compare between specific candidate sites to compare the relative robustness of each fracture system against the uncertainty parameters.



**Figure 8 A,B:** Tornado plot showing the sensitivity of pore pressure to slip for two fracture planes at the 4850 site against the uncertainties in individual input parameters. For example, Fault#1 seems to be most sensitive to a  $\pm 20^\circ$  variation in strike of the plane and Fault#2 seems to be most sensitive to  $\pm 0.1$  psi/ft variation in  $S_{hmin}$  magnitude. **C:** The orientation of the fault planes represented by a stereo-net plot with the inward gray arrows representing the  $S_{Hmax}$  azimuth. The difference in sensitivity of the fault planes to the parameters are due to the variation in orientations with respect to  $S_{Hmax}$ .

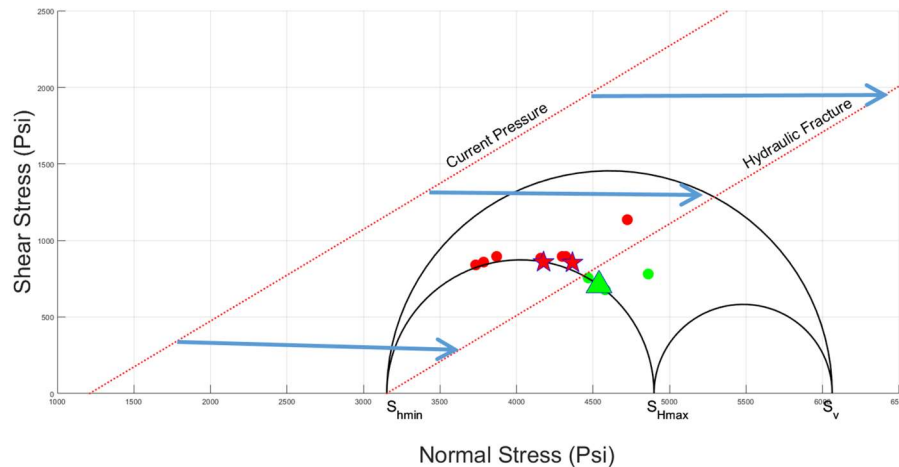
#### 4. Shear stimulation observations in Experiment 1

Although Experiment 1 was focused on stimulation to create planar hydraulic fractures, significant shear stimulation and creation of flow pathways may have occurred over the course of several stimulation and flow tests (Schoenball et al., 2019; Neupane et al., 2019). Evidence for likely shear stimulation in the Experiment 1 testbed includes the distribution of microseismic events, flow out of multiple zones in observations wells, Distributed Temperature Sensing (DTS) signals from locations of intersections of monitoring wells and natural fractures and inflow jets observed in production wells indicating flow from natural fractures (Neupane et al., 2019, Fu et al., 2019). Figure 9 shows the configuration of these signatures and the major natural fractures zones that resulted in creation of large flow pathways from shear stimulation. These zones include 1) Intermediate NF zone, 2) PDT-I connector, 3) PDT-OT connector and 4) OT-P connector. These connecting zones are consistent with the large fracture zones described in Figure 2 from the common DFN modeling exercise. In addition to these large zones, the natural fractures corresponding to the inflow locations at wellbores have been mapped from DTS signals and inflow jets along natural fractures.



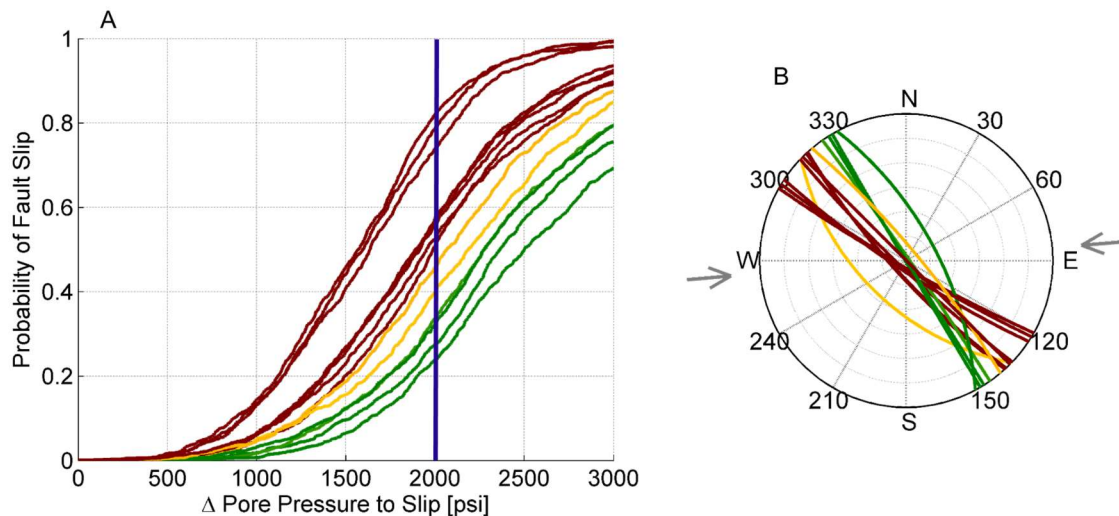
**Figure 9** 3D plot highlighting the activation of natural fractures over time during Experiment 1 (Neupane et al., 2019). The injection well is shown as the green line, monitoring wells as the yellow line and production well as the red line. The large blue spheres are the notch locations where the fluid injection experiments have been conducted. The small color coded spheres are the microseismic event locations colored by time of occurrence. The large red and purple spheres are the DTS signals from monitoring wells associated with the two locations: the shallower 142 ft notch and the deeper 164 ft notch. The large blue-gray disks are the inferred activated natural fracture zones in response to the fluid injection. Extensive details of these observations are given by Neupane et al. (2019).

Figure 10 shows the fracture planes with interpreted shear slip in Experiment 1 on a Mohr circle plot. Most of these planes are well oriented for shear slip at pressures lower than hydraulic fracture propagation, indicated by the position left of the hydraulic fracture failure line. Some of the planes plot in the stable zone, but their position is very close to the failure line. Considering the uncertainties in the stress state and fracture orientations, the shear slip observations and the slip tendency analysis show a reasonable overall agreement. The slip tendency analysis therefore provides a coherent explanation for the shear slip events from the geophysical monitoring data.



**Figure 10** Slip tendency of the planes interpreted to have experienced shear slip during Experiment 1 is plotted with a Mohr circle representation. The circles are the planes observed from well bore signals, i.e. DTS and flow jets. The stars and triangle are the large fracture zones shown in Figure 9. Most of the fracture planes seem to have a high slip tendency as indicated by the position in the Mohr circle to the left of the enhanced failure line, while the fractures that plot in the stable zone are very close to the failure line.

Figure 11 shows the probabilistic analysis for these fracture planes. The uncertainty parameters are the same as indicated in Table 2. Most of the planes have a very high probability of slip ( $>0.6$ ) at hydraulic fracture pressure indicated by the blue line. The fractures plotting in the stable zone in Figure 10 also have reasonable probabilities of slip between 0.3-0.4.



**Figure 11 A.** CDF curves for the fracture planes with inferred shear failure in Experiment 1. Most of the fractures have a very high probability of slip ( $>0.6$ ) at pressures required for hydraulic fracture formation (blue line). Even the fractures classified as stable in Figure 10 have a reasonable slip probability between 0.3-0.4. **B.** The fractures plotted in the stereo-net representation. The fractures with a high probability of shear slip are steeply dipping with a strike around  $300^\circ$ .

#### 4. Stochastic evaluation of potential shear stimulation at 4100

As mentioned, the 4100 level is being evaluated as a potential site for achieving the shear failure objectives of Experiment 2. Although characterization of the site is still preliminary, we have been

conducting initial analysis of the advantages of different potential borehole layouts. Specifically, we seek borehole orientations that increase the probability of intersection of the injector and producer wells with fractures that are prone to shear failure in response to injection.

For this analysis, we utilize a statistical treatment of the joint sets based upon prior fracture mapping (Figure 3 and Table 3). A complete review of borehole layout designs and associated evaluations is presented in Frash and Morris (2019). Here we present a subset of results to emphasize the interplay between borehole layout and joint set orientations that have high slip tendency. These analyses utilized the ‘Fat Crayon Toolkit’ that is in development for the EGS Collab Team and will soon to be made publicly available. This tool combines 3D (vtk) discrete fracture network creation and borehole geometry with statistical analysis of fracture intersections and slip tendency. The toolkit is intended to aid evaluation of borehole layouts for field sites. Figure 12 shows two potential borehole layouts with ‘A’ having more slanted injection/production boreholes compared with ‘B’. Figure 13 shows the corresponding analysis of the intersection and shear activation of one stochastic realization for each of the three joint sets. Deterministic fracture networks using drift and borehole data are planned in future work. The preliminary results indicate that layout ‘A’ is more likely to intersect and activate JS2, while layout ‘B’ is more likely to intersect and activate JS3.

**Table 3: Summary of previously mapped joint sets in the 4100 area.**

Fracture Set Data	Strike; Azn (deg)	Dip (deg)	Source
JS1	15 ±15	35 ±5	Hladysz, 2009
JS2	260 ±30	69 ±15	Hladysz, 2009
JS3	120 ±40	35 ±30	Hladysz, 2009

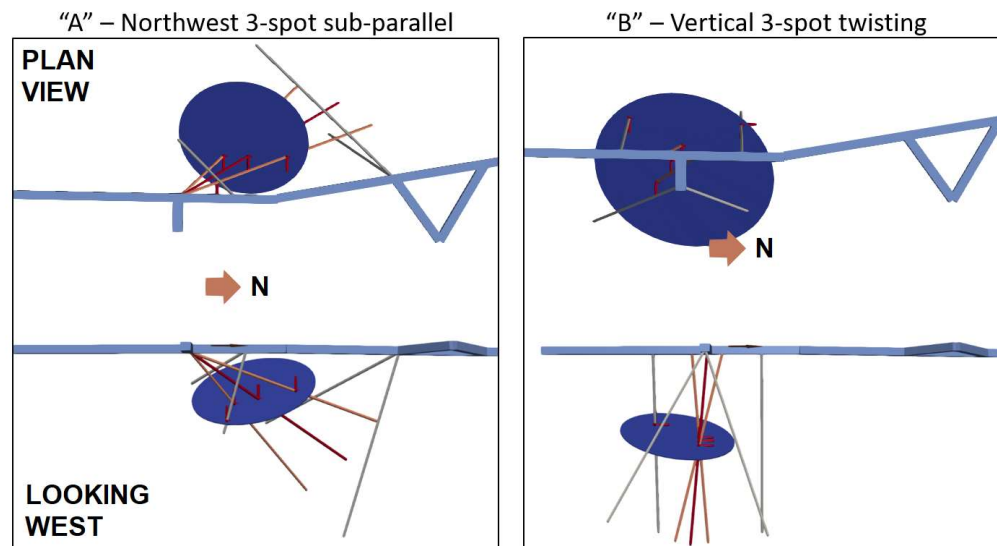


**Figure 12: Two potential borehole layouts for the Experiment 2 test bed which include an injector (red), two producers (orange), monitoring boreholes (grey), drifts (light blue), and an example fracture intersecting the injection well (dark blue disk).**

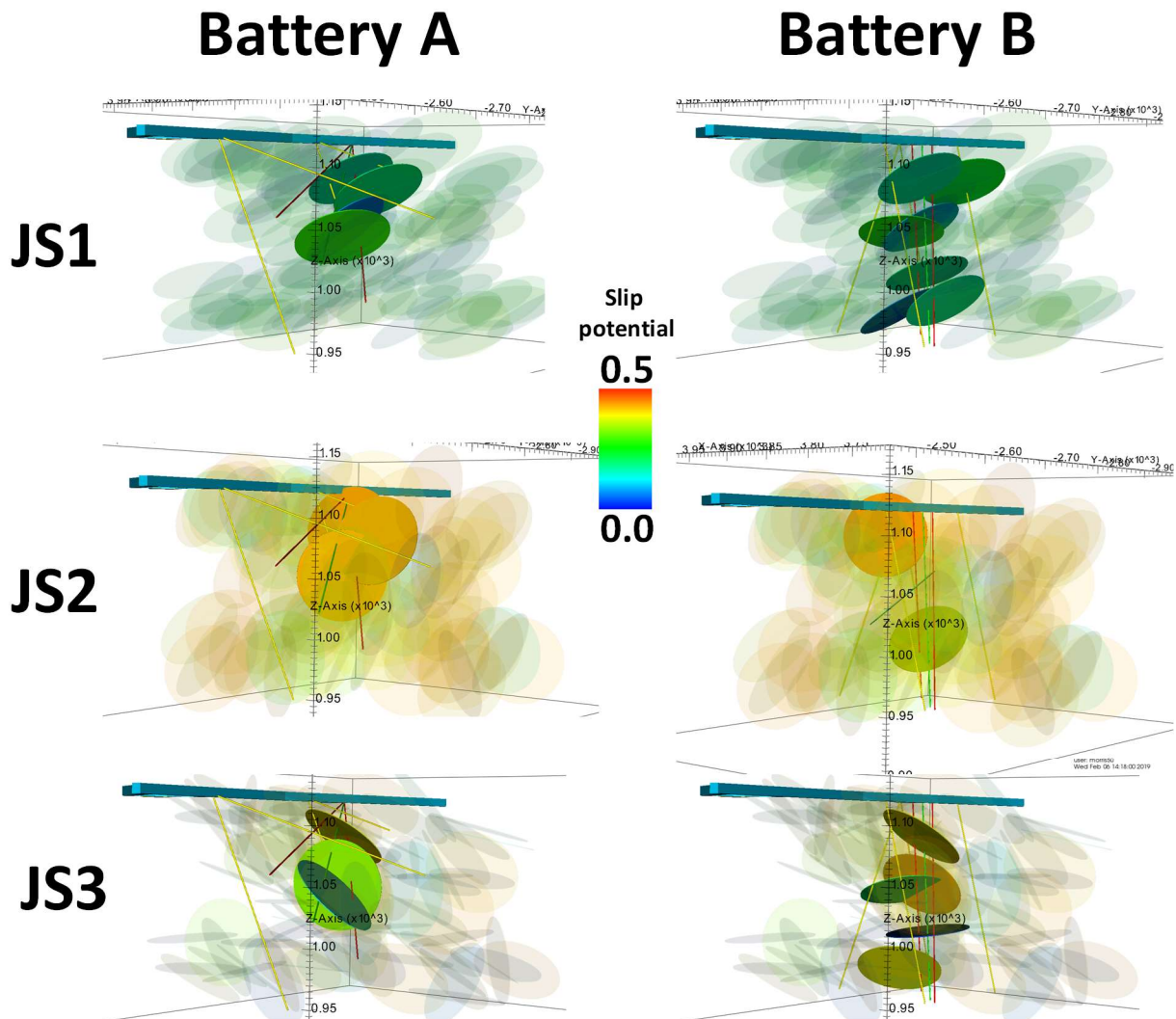


Figure 13: Example visualization using the 'Fat Crayon Toolkit' to evaluate layouts 'A' and 'B'. These figures highlight the propensity for slip in hot colors, and linkage of injector/producer pairs with opacity. That is, we seek scenarios where we have many opaque, red fractures. The sub-vertical orientation of the injection and production wells associate with many potential natural fracture intersections and many of these randomly distributed fractures are oriented favorably for hydroshearing (JS2 and JS3). Specifically, it appears that the layout 'A' is more likely to intersect and activate JS2, while layout 'B' is more likely to intersect and activate JS3.

## 5. Conclusions: Inputs into site selection

The analysis of the fracture configuration and slip tendency is an important input for Experiment 2 site selection. Observations from Experiment 1 have shown that extensive shear stimulation has taken place in response to fluid injection, resulting in the creation of multiple flow paths. The planes interpreted to have experienced shear failure from the geophysical monitoring data are generally consistent with the predicted slip tendencies. This highlights the importance of characterizing the stress state and modeling shear failure for Experiment 2. The observations of shear failure in Experiment 1 and slip tendency analysis for the inferred planes shows that the

interpreted stress state in the area is consistent with shear failure observations and a simple Coulomb failure analysis can predict the planes that are likely to slip in response to fluid injection.

The present analysis shows the presence of fault/fracture planes optimally oriented for shear stimulation at both the candidate sites. From the present analysis, the optimal target fractures for shear stimulation at the two sites are:

1. NW-SE striking near vertical fractures at the 4850 site: These are proven targets based on Experiment 1 results and the slip tendency analysis.
2. E-W striking near vertical fractures (JS2) at the 4100 site: These fractures have high shear slip potential and will be prime targets, if encountered in the planned boreholes. The foliation parallel features at this site are not good candidates and have extremely low shear slip tendency.

The major differences between the two candidate sites are:

1. **Current state of test bed:** Due to the existing shear stimulation at the 4850 site, leakage pathways exist at the 4850 site while the 4100 location presents an opportunity to perform the test in an undisturbed state.
2. **State of characterization:** The 4850 is already well characterized in terms of stress state and fracture networks from boreholes with multiple orientations and drift mapping. The 4100 characterization is limited to drift wall mapping only.
3. **Lithology:** The 4100 site potentially provides a less complicated test bed in terms of compositional heterogeneity compared to the 4850. However, this needs to be verified from core observations from wellbores.

The way forward includes:

1. Stress characterization program at the 4100 site to confirm if the stress state is consistent with the stress model of the 4850 site.
2. DFN characterization at the 4100 site similar to the 4850 CDFN program utilizing multiple borehole observations to characterize the fracture network.
3. Slip tendency analysis for specific shear stimulation targets at the 4100 and 4850 sites including an uncertainty analysis to rank the sites in terms of favorability for shear stimulation.

## Acknowledgements

This material was based upon work supported by the U.S. Department of Energy, Office of Energy Efficiency and Renewable Energy (EERE), Office of Technology Development, Geothermal Technologies Program, under Award Number DE-AC02-05CH11231 with LBNL and other subcontracts. The United States Government retains, and the publisher by accepting the article for publication, acknowledges that the United States Government retains a non-exclusive, paid-up, irrevocable, world-wide license to publish or reproduce the published form of this manuscript, or allow others to do so, for United States Government purposes. The research supporting this work took place in whole or in part at the Sanford Underground Research Facility in Lead, South Dakota. The assistance of the Sanford Underground Research Facility and its personnel in providing physical access and general logistical and technical support is gratefully acknowledged; we thank

Kathy Hart and Jaret Heise for providing geologic maps of the Homestake Mine. The hydrostructural model was created using Golder's FracMan software. The earth model output of the fractures was generated using Leapfrog Software. Copyright © Seequent Limited. Leapfrog and all other Seequent Limited product or service names are registered trademarks or trademarks of Seequent Limited.

## REFERENCES

- Caddey, S.W., Bachman, R.L., Campbell, T.J., R.R. Reid, and Otto R.P. "The Homestake Gold Mine, An Early Proterozoic Iron-Formation-Hosted Gold Deposit, Lawrence County, South Dakota." *U.S. Geological Survey Bulletin* 1857-J, Geology and Resources of Gold in the United States, (1991), 67 pp.
- Condon, K., Sone, H., Wang, H.F. and the EGS Collab Team "Influence of Foliation Orientation on Rock Strength and Elastic Properties of Poorman Schist from the EGS Collab Experiment 1 Site." *AGU Fall Meeting*, (2018), H11Q-1693.
- Dobson, P., Kneafsey, T., Morris, J., Singh, A., Zoback, M., Roggenthen, W., Doe, T., Neupane, G., Podgorney, R., Wang, H., Knox, H., Schwering, P., Blankenship, D., Ulrich, C., Johnson, T., White, M., and the EGS Collab team "The EGS Collab hydroshear experiment at the Sanford Underground Research Facility – Siting criteria and evaluation of candidate sites." *Geothermal Resources Council Transactions*, **42**, (2018), 708–723.
- Frash, L.P., Carey, J.W., Welch, N.J., and the EGS Collab Team. "EGS Collab Experiment 1: Geomechanical and hydrological properties by triaxial direct shear." *Proceedings, 44<sup>th</sup> Workshop on Geothermal Reservoir Engineering*, Stanford University, SGP-TR-214, (2019), 11 p.
- Frash, L.P., Morris, J.P., and the EGS Collab Team, "Stochastic prediction of multi-well fracture connectivity and application to EGS Collab experiment 2." ARMA 19–1823, *Proceedings of the 53rd US Rock Mechanics/Geomechanics Symposium held in New York, NY, USA, 23–26 June 2019*.
- Fu, P., Schoenball, M., Morris, J., Ajo-Franklin, J., Knox, H.A., Kneafsey, T.J., Burghardt, J., White, M., and the EGS Collab Team. "Microseismic signatures of hydraulic fracturing: a preliminary interpretation of intermediate-scale data from the EGS Collab Experiment." *Proceedings 44th Workshop on Geothermal Reservoir Engineering*, Stanford University, Stanford, California, (2019).
- Hart, K., Trancynger, T.C., Roggenthen, W., and Heise, J. "Topographic, geologic, and density distribution modeling in support of physics experiments at the Sanford Underground Research Facility (SURF)." *Proceedings of the South Dakota Academy of Science*, **93**, (2014), 33–41.
- Hladysz, Z.J. "Development of a 3-D structural geology model of Homestake's 4100 to 5000 levels at the proposed location of the large cavities." SDSMT CONTRACT #09-05, (2009).
- Kneafsey, T.J., Dobson P.F., Ajo-Franklin, J.B., Guglielmi, Y., Valladao, C.A., Blankenship, D.A., Schwering, P.C., Knox, H.A., White, M.D., Johnson, T.C., Strickland, C.E., Vermuel V.R., Morris, J.P., Fu, P., Mattson, E., Neupane, G., Podgorney, R.K., Doe, T.W., Huang, L.,

- Frash, L.P., Ghassemi, A., Roggenthen, W., and the EGS Collab Team. "EGS Collab Project: Status, Tests, and Data." ARMA-19-2004, (2019a), 21 p.
- Neupane, G., Podgorney, R.K., Hunag, H., Mattson, E.D., Kneafsey, T.J., Dobson, P.F., Schoenball, M., Ajo-Franklin, J.B., Ulrich, C., Schwering, P.C., Knoz, H.A., Blankenship, D.A., Johnson, T.C., Strickland, C.F., Vermuel, V.R., White, M.D., Roggenthen, W., Uzunlar, N., Doe, T.W., and the EGS Collab Team. "EGS Collab Earth Modeling: Integrated 3D Model of the Testbed" *GRC Transactions*, 43, 22p.
- Lu, J., and Ghassemi, A. "Coupled thermo-hydro-mechanical-seismic modeling of fracture reservoir simulation with application to EGS Collab." *Proceedings, 44<sup>th</sup> Workshop on Geothermal Reservoir Engineering*, Stanford University, SGP-TR-214, (2019), 13 p.
- Oldenburg, C.M., Dobson, P.F., Wu, Y., Cook, P.J., Kneafsey, T.J., Nakagawa, S., Ulrich, C., Siler, D.L., Guglielmi, Y., Ajo-Franklin, J., Rutqvist, J., Daley, T.M., Birkholzer, J.T., Wang, H., Lord, N.E., Haimson, B.C., Sone, H., Vigilante, P., Roggenthen, W.M., Doe, T.W., Lee, M.Y., Ingraham, M., Huang, H., Mattson, E.D., Zhou, J., Johnson, T.J., Zoback, M.D., Morris, J.P., White, J.A., Johnson, P.A., Coblenz, D.D., and Heise, J. "Intermediate-Scale Hydraulic Fracturing in a Deep Mine, kISMET Project Summary 2016." Lawrence Berkeley National Laboratory, Report LBNL-1006444, (2016), 114 p.
- Pariseau, W.G. "Research Study on Pillar Design for Vertical Crater Retreat (VCR) Mining." *US Bureau of Mines Open-File Report 44-86*, NTIS PB86-210960, (1986), 232 pp.
- Schoenball, M., Ajo-Franklin, J.B., Blankenship, D., Cook, P., Dobson, P., Guglielmi, Y., Fu, P., Kneafsey, T., Knox, H., Petrov, P., Robertson, M., Schwering, P., Templeton, D., Ulrich, C., Wood, T., and the EGS Collab team. "Microseismic monitoring of meso-scale stimulations for the DOE EGS Collab project at the Sanford Underground Research Facility." *Proceedings, 44th Workshop on Geothermal Reservoir Engineering*, Stanford University. (2019), 8 p.
- Schwering, P.C., Blankenship, D., Podgorney, R.K., Neupane, G.H., Doe, T., Ulrich, C., Dobson, P.F., Kneafsey, T.J., Singh, A., Smith, M.M., Roggenthen, W., Uzunlar, N., and EGS Collab Team. "The First EGS Collab Testbed at the Sanford Underground Research Facility – Discrete Fracture Network Characterization." *AGU Fall Meeting*, (2018), H32C-06.
- Stedman, J.A., and Large, R.R. "Synsedimentary, Diagenetic, and Metamorphic Pyrite, Pyrrhotite, and Marcasite at the Homestake BIF-Hosted Gold Deposit, South Dakota, USA: Insights on Au-As Ore Genesis from Textural and LA-ICP-MS Trace Element Studies." *Economic Geology*, 111, (2016), 1731–1752.
- Stetler, L.D. "Water Geochemistry and Pressure Buildup in Drill Holes on the 4850-Ft Level at the Sanford Underground Research Facility." *Proceedings of the South Dakota Academy of Science*, 94, (2015), 317–327.
- Ulrich, C., Dobson, P.F., Kneafsey, T.J., Roggenthen, W.M., Uzunlar, N., Doe, T.W., Neupane, G., Podgorney, R., Schwering, P., Frash, L., Singh, A., and the EGS Collab team. "The distribution, orientation, and characteristics of natural fractures for Experiment 1 of the EGS Collab Project, Sanford Underground Research Facility." *Proceedings, 52nd US Rock Mechanics / Geomechanics Symposium*, ARMA 18-1252, (2018), 8 p.
- Vigilante, P.J. "Critical Review of Laboratory Rock Properties and State of Stress in the Sanford Underground Research Laboratory (SURF)." Unpublished kISMET report. (2016), 51 p.

- Vigilante, P.J., Sone, H., Wang, H.F., Haimson, B., and Doe, T.W. "Anisotropic strength of Poorman Formation rocks, kISMET project." *Proceedings, 51<sup>st</sup> US Rock Mechanics / Geomechanics Symposium*, ARMA 17-766, (2017), 6 p.
- Walsh, F.R.I., Zoback, M.D., Pais, D., Weingartner M., and Tyrell, T. "FSP 1.0: A program for probabilistic estimation of fault slip potential resulting from fluid injection." (2017), <http://scits.stanford.edu/software>
- Wang, H.F., Lee, M.Y., Doe, T.W., Haimson, B.C., Oldenburg, C.M., and Dobson, P.F. "In-situ stress measurement at 1550-meters depth at the kISMET test site in Lead, S.D." *Proceedings, 51<sup>st</sup> US Rock Mechanics / Geomechanics Symposium*, American Rock Mechanics Association, ARMA 17-000651, (2017), 7 p.
- White, M.D., Fu, P., Ghassemi, A., Huang, H., Rutqvist, B., and Johnston, B. "Numerical Simulation Applications in the Design of the EGS Collab Experiment 1." *Proceedings, 43<sup>rd</sup> Workshop on Geothermal Reservoir Engineering*, Stanford University, SGP-TR-213, (2018).
- Zoback, M.D., Lund Snee, J.E. "Predicted and observed shear on pre-existing faults during hydraulic fracture stimulation." SEG international Exposition and 88th Annual Meeting Expanded Abstracts, 10.1190/segam2018-2991018.1, (2018), p. 3588.